2024-01-12

Process parameter optimisation for Waspaloy using Laser-Directed Energy Deposition with Powder

Johannes Lövhall

BACHELOR'S THESIS
Mechanical Engineering
Department of Engineering Science

Acknowledgments

The advisory support provided by Fabian Hanning at University West has been greatly appreciated.

Abstract

Material utilisation is of importance in the manufacturing industry for making the most of each material, minimising waste and increasing cost-effectiveness. In this thesis, samples of Waspaloy built with the method of L-DED-P has been analysed in order to investigate how process parameters influence the build quality and geometrical accuracy in as-built objects. The samples analysed was built in single rows of one, three, five and fifteen layers. A build process was used in which the samples were built with individual combinations of the process parameters laser power, scanning speed, and powder flow. Each combination of process parameters was used to build one track for each layer height.

Analysis included defect analysis with light optical microscopy, and post-processing with ImageJ for automatic identification, quantification, and collection of measurements. A qualitative analysis was performed and the sample properties and characteristics was described in terms of the amount of defects, including a descriptive assessment of defect severity. Etched samples revealed a columnar grain structure in samples, which was apparent in builds with at least three layers.

The results presented show a difference in build height, quantity and size of pores, and the presence or absence of other defects such as lack of fusion. Sample 3 which was built with high laser power, slow scanning speed, and high powder feed show promising results with one of the highest build rates of all samples, combined with a low normalised pore distribution. The sample experiences partial hardening, with hardness values reaching 320 HV, but still promisingly show no sign of crack formation.

It is concluded that powder feed relates primarily to the build rate of the samples, and the scanning speed together with the laser power influence the quality of the build, where high laser power and low scanning speed tends to form well behaving samples with few defects, whilst other combinations increase the risk of defects.

Date:	2024-01-12
Author:	Johannes Lövhall
Examiner:	Joel Andersson
Advisor:	Fabian Hanning (University West)
Programme name:	Mechanical Engineering
Main field of study:	Mechanical engineering
Course credits:	22.5 HE credits
Publisher:	University West, Department of Engineering Science, S-461 86 Trollhättan, SWEDEN

Contents

Nomenclature

3D	=	Three dimensional or three dimensions
AM	=	Additive Manufacturing
DED	=	Direct Energy Deposition
FCC	=	Face Centered Cubic
LMD	=	Laser Metal Deposition
L-DED	=	Laser-Directed Energy Deposition
L-DED-P	=	Laser-Directed Energy Deposition with Powder
LOM	=	Light Optical Microscopy
MRO	=	Maintenance and Repair Operations

1 Introduction

Our modern world depends upon industrial scale manufacturing, producing products in an ever increasing rate, to an ever increasing demand. Countries globally are working towards a world of manufacturing where customer demand is constantly met. Corporations and industry nations are competing in an international arena, for customers all over the globe. Internet has created a global trading arena in which companies can reach previously unattainable markets [1]. Increased competition puts companies in a position where innovation is essential for survival, and adopting new strategies are key for sustainable prosperity. Manufacturing has traditionally been dependent on subtracting manufacturing. In subtracting manufacturing, there is an adherent waste continuously generated throughout the process of producing a part. Producing means subtracting – removing – material from a large piece of untreated and -processed material. To manufacture a part with correct geometry and design within shape and surface tolerances, the material needs to be processed in multiple subsequent steps. Resource efficiency is key to optimize use of available materials and use what resource already available to the maximum, and optimum, extent. However, the subtracting approach is inherently a wasteful process, and can be optimised only so much.

Additive Manufacturing (AM) is an alternative approach in manufacturing. Contrary to traditional manufacturing, the AM method is producing parts by adding material layer by layer. AM can enable the production of complex geometries with minimal waste, making it a promising manufacturing method [2]. From an industry perspective, AM offers a new way to optimise manufacturing. With the technology, previously too complex designs are now possible to produce.

Maintenance and repair operations (MRO) is an area where AM can be a key player in realizing locally produced replacement parts, or even to repair a worn component in-situ [2]. Embracing AM means selecting a technology in development. Adoption to an industry setting requires customizing and tweaking from end-users to experimentally find adequate process parameters. Proper and efficient use of AM requires trained personnel, with thorough understanding of how the process works and how to choose production parameters. Finding reliable process parameters in AM is one of many challenges in making the process more attractive in industry [3].

As technology matures, it is expected that investment cost decreases, further enabling a quicker adoption rate within industry, and an accelerated rate of technology development as know-how for the processes are spread wide [4].

1.1 Purpose

The aim for the thesis is to investigate how the choice of process parameters in Laser-Directed Energy Deposition with Powder (L-DED-P) using Waspaloy affects build geometry, formation of defects, and hardness. Finding reliable process parameters requires the L-DED-P process to achieve a high level of geometrical accuracy, with a minimum defects such as cracks. Grain size and growth is also to be investigated as part of the analysis.

1.2 Delimitations

An experimental research approach should normally include an experimental phase. In this thesis, due to limitations in time and resources, the design and manufacturing of samples are outside the scope. Observation of the manufacturing process is included as means of understanding the process and the method for how the samples are produced.

Within the scope of the thesis are the following points:

- Analysis of prebuilt samples
- Cutting and preparing samples
- Hardness testing of samples
- Microstructural analysis with light optical microscopy (LOM)

The analysis of samples is primarily limited to the use of LOM for investigating the samples. Physical material properties are limited to hardness testing using the Vickers method.

2 Theoretical framework

Theory is presented with a focus on presenting a broad overview on superalloys and Waspaloy with the goal of pinpointing a current state of research. The theoretical framework covers a general description of superalloys, which is followed by a presentation of Waspaloy. A look into AM and L-DED concludes the section.

2.1 Superalloys

All materials are not created equal, this applies especially to metals and alloys. Engineering ingenuity has created materials with high resistance to mechanical stress and strain, as well as against high temperature material creep and deformation. A common application is in jet engines where components are subject to high temperatures and stress. The conditions inside of an jet engine require use of materials which can handle high stress in high temperatures, for an extended period of time.

In high temperature environments, it is crucial for components to withstand the heat without having the physical geometry and/or material properties change and diverge from manufactured specification. A high temperature superalloy is classified as an alloy withstanding and being fit for application in temperatures near its critical melting point. In general, a baseline for classification is set as the condition $T_o > 0,6\dot{T}_m$ for a melting temperature T_m, and an operating temperature T_o. The criterion indicates that the material should withstand load during operation in temperatures near its melting temperature. Rearranging the criterion gives a quotient, the homologous temperature, that is defined as $\tau = T_o/T_m$, where $0 <= \tau <= 1$ with theoretical extremes corresponds to $T_o = 0$ and $T_o = T_m$ respectively. The temperature is measured and calculated in unit Kelvin.

Different production methods and materials promote alternative types of crystal structures. Equiaxed crystal structure is a structure in which grains

grows independently, in all directions, creating a surface area with grains of varying shapes and dimensions. Boundaries are formed in between grains which separates one grain from another. A columnar structure is produced by using a method of directional solidification, which occurs naturally in the process of L-DED due to the thermal gradient between layers in the vertical axis, and the scanning direction along a horizontal axis. The grain structure is ordered in columns, where a predominant feature is grains that are stretched lengthwise. Just as in the equiaxed case, the grains are separated by boundaries. In addition to equiaxed and columnar structured crystals, there is also single crystal structure. The single crystal have ordered arrangement of atoms throughout the whole of the material volume [5]. A single crystal lattice is grown continuously to a predetermined limit. Boundaries are not present, which gives the material unique properties, such as improved mechanical properties.

2.1.1 Types of superalloys

There are primarily four groups of high temperature alloys [6]. Each group is named after which material that plays the major role in the composition. The four categories are:

- Iron
- Iron-nickel
- Nickel
- Cobalt

Superalloys was born with the idea of creating an alloy with only the best properties from each of the constituent components, beginning in the first half of the 20th century, with iron-based alloys. Iron was the primary source material for creating alloys in the early 20th century. The primary use of iron came from experimenting with compositions to improve properties of steel. Steel is an alloy, created by adding carbon to iron, and compared to iron, it has superior strength. In room temperature and low temperatures, the steel has excellent mechanical properties suitable for a variety of applications, such as in construction material, in cars, and in kitchen knives. By modifying the amount of carbon, different properties can be attained. The idea of adding more components in addition to carbon for an even better performance was not far fetched, and gained traction especially with the inception of World War 2 and the need for ever better materials [7].

A common goal for the superalloys, regardless of type, is the desire to achieve and maintain high strength, low creep-fatigue, and resistance against oxidation in high temperature applications. Whether a superalloy is based on iron, iron-nickel, nickel or cobalt, it is the mechanical properties and resistance to wear, creep, and oxidisation that is a striving force for continued research. Nickel-based superalloys can offer a higher homologous temperature than other types of superalloys [7], [8], making it a preferred choice in high temperature applications.

2.1.2 Phases

Superalloys are designed to utilise a FCC (Face Centered Cubic) crystal lattice structure. A primary γ austenitic phase is found in superalloys, and in addition,

Table 1: *Phases of superalloys and information in which types of superalloys they are found, and which lattice structure that are represented [7], [9]. Body Centered Tetragonal (BCT) structure is seen in phase γ'', and Hexagonal Closest Packed (HCP) in phase η. Phase δ shows an orthorhombic structure.*

Phase	Commonly represented in superalloy types	Crystal structure
γ	All	FCC
γ'	Nickel and iron-nickel	FCC
γ''	Inconel 718 (Nickel based material)	BCT
δ	Nickel and iron-nickel	Orthorhombic
η	Iron-nickel, nickel and cobalt	HCP

multiple secondary phases pertaining to γ' (gamma-prime), γ'' (gamma-double-prime), η and δ [7]. The phase designation represents a specific type of lattice structure, specified in Table 1.

Precipitation hardening theory states that the precipitate particles restricts the dislocation mobility in the matrix. A description of phases and carbides is presented below:

Carbides: Formed by carbon combining with reactive elements, and usually forms in the vicinity of grain boundaries. Primary carbide of the form MC tends to decompose to form other forms of carbides during heat treatment processing or during use in elevated temperatures. Due to the formation of carbides in the grain boundaries, the protection against grain boundary sliding is increased enhancing the strength of the material, while still allowing ductility formed from the precipitates of other phases.

Gamma phase: A phase in which other phases reside. It has a FCC structure, and contributes to the total material strength via solid solution hardening [10]. Materials rhenium, ruthenium, molybdenum, chromium prefer this phase [8].

Gamma prime phase: Is a precipitate complementing the gamma phase. It too has a FCC crystal structure. Materials in this phase are nickel, aluminum, titanium and tantalum [8]. Creep strength is particularly related to the proportion of γ' in precipitation-hardened alloys [8].

Gamma double prime phase: Superalloys of nickel(-iron)-base containing niobium will have primary strengthening in this precipitation phase. The structure is BCT [8].

2.1.3 Heat treatments

Superalloys material composition may be tweaked for custom applications, enhancing properties, on behalf of reducing other properties. A superalloy does not become *super* simply with the correct compound of materials, but a significant part of creating the material is in the production method, and in the post-processing. Heat treatment is in an umbrella term relating to processes which are used to regrow grains in a structured and systematic manner.

Age-hardening, also known as precipitation hardening, is a method for increasing the strength of a material by introducing small uniformly scattered particles, precipitates, in an already existing, primary phase [11]. The primary

phase for nickel-based superalloys is $\$gamma$, with a γ' secondary phase for hardening, with the exception for Alloy 718 which uses the metastable γ'' [12]. The precipitates inhibit movement of dislocations, which is the reason for the increased strength and hardness.

The method requires that there exists a maximum solubility limit of one component in the other, and that the solubility quickly decreases with temperature recession. Also, the age hardened alloy must have a precipitate composition less than the maximum solubility [11]. Additionally, a heat treatment in two steps is required to achieve success:

1. Heating the alloy to a temperature in which all solute are dissolved into a single phase. When there is only a single phase present at the elevated temperature, and the soluble phase has dissolved, oversaturating has now occurred and the material is quenched. The rapid cooling prevents formation of an unwanted phase, retaining the oversaturation. The process is called solution heat treatment, as it is solving a phase in another.

2. After the solution heat treatment, the first phase is oversaturated and in a nonequilibrium state. Precipitation heat hardening is the process in which the solved phase begins to grow precipitates within the alloy [11]. As mentioned, the precipitates are uniformly dispersed, and as the precipitates form, the alloy is hardened in a process called aging. Aging is a process dependent on time and temperature. Strength increases with time, up to a limit. Strengthening in the aging process follows the approximate shape of a negative parabola. A positive relation between time and strength is seen at first, until a maximum strength is reached. After this point and onward, the alloy has been overaged, and the relation between strength and time is now negative, with decreasing strength with increasing time.

In addition to solution-treating and age-hardening, there are complementary heat treatment methods available.

Stress is built into the material as it is being worked, and methods for relieving the energy are necessary to achieve ductility in order to work and shape the material. Two processes for stress-relieving are “full annealing” and “in-process annealing”.

Full annealing serves the purpose of recrystallising the alloy, increasing ductility. The process is especially important as a preprocessing step in before machining, forming or welding. Full annealing is also useful only for full recrystallise, even if it is not for the purpose of further shape forming.

In-process annealing is used for annealing during process in which the material is successively shaped into a net-shape. In shaping and forming, energy is stored within the material, and as the energy increases, so does the risk of failure and cracks. Mitigating risk of material failure is to anneal in-process, as intermediate steps in the shaping process. Both cold and hot working benefits, although cold working often is performed on solution-treated, not yet age hardened, material. Annealing process temperature and procedure is dictated by working practice, the desired regrowth, and recrystallisation grade.

2.2 Waspaloy

Waspaloy is a registered trademark superalloy where the composition can vary depending on the exact purpose of use and application. Standards AMS 5828

Table 2: *Nominal composition of Waspaloy according to standard AMS 5828 and AMS 5596 respectively [13].*

	Waspaloy composition in wt%
B	0.003 - 0.010
Zr	<0.04
C	0.02 to 0.10
Cu	<0.10
Mn	<0.10
P	<0.10
S	<0.10
Si	<0.10
Al	1.20 to 1.60
Fe	<2.00
Ti	2.75 to 3.50
Mo	3.50 to 5.00
Cr	18.00 to 21.00
Co	12.00 to 15.00
Ni	Balance

and AMS 5596 refer to Waspaloy, and are provided by Society of Automotive Engineers (SAE) under the category of Aerospace Material Specifications (AMS). A material composition is provided in Table 2.

2.2.1 Classification

Waspaloy is a polycrystalline nickel-based superalloy strengthened by gamma prime phase γ' [13], [14]. As it is mainly γ' that provides the strength, the alloy is classified as a precipitation hardened nickel based superalloy.

2.2.2 Forming, heat treatments and strength

Predominantly, the material is wrought or cast to a near net-shape, after which post-processing and machining is performed for touch-up and finalising the shape. Forming can be done in hot or cold state. Hot forming typically requires a temperature at or above 1040°C [15]. According to Utada et al. [14] the amount of present γ' rapidly decreases around 1000°C. At 1044°C, γ' has completely dissolved into γ.

According to Haynes® [15], heat treatment is done in four steps. First, a priming solution annealing at temperatures around 1070 °C with subsequent quenching. Then follows a three step age hardening procedure, where the material is subjected to 996 °C for 2 hours, 843 °C for 4 hours and 760 °C for 16 hours with air cooling between each step.

Due to the mechanical properties, the material has been a popular choice within the aerospace industry, as a material suitable for use in the hot section of jet engines. The material has high strength at high temperatures, and has high strength retention up to about 650 °C. By linearising the data from Table 3, the mean decline of strength per degree from 649 °C to 982 °C is −2.89 MPa/°C.

Table 3: *Ultimate tensile strength of Waspaloy from data received from Haynes® datasheet [15].*

Temperature °C	Ultimate tensile strength [MPa]
Room temperature	1304
204	1263
427	1183
538	1175
649	1137
760	822
816	633
871	456
927	297
982	174
1093	51

2.2.3 Cracks and defects

Weldability of Waspaloy is poor [13], [16], and the superalloy is drawn with challenges in regards to cracking. Cracking however, can occur in different ways, and by different means. Hot cracking occurs due to reactions in the microstructure due to thermal gradients invoked in a welding operation. The cracking is categorised in two primary categories: solidification, or heat affected zone cracks [16].

Solidification cracks occurs in melt pool during solidification, while liquation cracks primarily occurs in the heat affected zone (HAZ). Cracks form in an solidification process where the melt pool is in a semi-solid state. The solidification invokes formation of dendrite structures that hinders liquid from flowing to interdendritic areas [17]. A lack of liquid in the dendritic network results in hot tears.

Strain-age cracks occur during reheating to the aging temperature. Formation of γ' precipitates is quicker than the relaxation of stresses. While the precipitation increases strength, it also induces higher stress in the material, which adds to previous residual stresses. Cracks forms if the induced stress from the new formation of precipitates exceeds the ductility limit [17].

Geometrical defects and damages in microstructural integrity by cracks and pores are areas that cause the material to not be able to perform optimally. Markanday [18] has investigated the phenomena and problem of cracking during use of AM. It is proposed that a tailored approach be used to create alloy design specific for use of AM would reduce the risk of defects arising. Appropriate deposition parameters and post-processing too can help in reducing crack formation, putting the responsibility on the AM-method and the build parameters. Methods for mitigating crack formation has been proposed, such as post-process reheating of the processed area. In-situ treatments have been investigated by Oh et al. [19] in an AM setting for reducing the formation of defects. It is shown that substrate heating performs better in reducing crack formation compared to post-heating. Additionally it is found that AM processing parameters are key for achieving good properties in subsequent layers, as material may otherwise be left unmelted, and unfused to the substrate or underlying layers.

2.3 Additive Manufacturing

Additive manufacturing is the process of manufacturing a part or component by building it layer by layer. AM is an umbrella concept, featuring multiple disciplines of varying production methods. Complex geometries and shapes difficult to attain with traditional manufacturing are possible to manufacture due to the additive approach [20]. Constructions with complex designs are possible to create, even with overhang and voids within the manufactured part. Flexibility in manufacturing allows for creative and optimised component designs, where computational optimisation may help reduce weight, whilst increasing strength and rigidity [20]–[22].

There are seven underlying types of AM processes; binder jetting, direct energy deposition (DED), powder bed fusion (PBF), sheet lamination, material jetting, vat polymerisation, and material extrusion [21]. Development of commercial 3D (three dimensional) printers has had an explosive rise, and availability of and range of commercial printers are broad and wide [23]. The high interest in the technology, has enabled cost of implementation to decrease, with available apparatus for both industrial and hobbyist use.

3D printers for private use often use material extrusion with fused deposition modelling (FDM) as the main feature of manufacturing. A part is printed layer by layer by feeding a filament wire into an extruder [22], where the filament is melted. As the filament has melted, it is deposited in a layer by layer fashion in order to gradually build the 3D-model [23]. The machines need only a source file in appropriate format from which it gathers print parameters and paths [22]. Printing is afterwards automatic. Printers in this area differentiates in resolution capability, the smallest possible increment in z-level, accuracy and possible error / fault handling.

2.3.1 Laser-Directed Energy Deposition (L-DED)

AM processes utilising direct energy deposition (DED) has come forth as an emerging and promising set of processes used in remanufacturing and refurbishing. A wire or powder is in this type of process fed directly into an energy source, where the powder or wire melts, and bonds to a substrate.

L-DED with powder, L-DED-P, uses a laser beam as the heat source. The laser is used on a substrate onto which the powder is to be bonded. A focused area on the substrate is hit by the laser beam, creating heat and in that, an interface where the substrate is melted, see Figure 1.

Powder is injected into the focus of the beam, at the surface of the melted substrate. Different nozzle designs can be used, giving various spray powder patterns. There are first the positioning of either in axis (coaxial position) or off-axis with the laser. Further segmentation comes

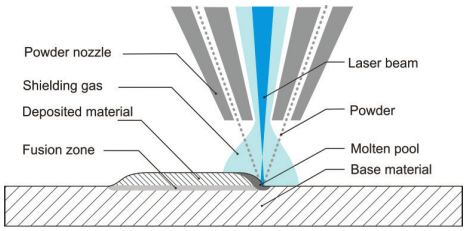

Figure 1: *Schematic of laser-directed energy deposition with powder. Powder injectors are coaxial with the laser beam, but this may differ between applications, and the injectors could also be placed off-axis. Shielding gas is used to reduce oxidisation and help with material bonding.* Laser Metal Deposition by [24], CC BY-NC-ND 3.0 Deed

from the choice of either a continuous
or discrete nozzle. A continuous nozzle provides an even distribution of powder in a cone-shape. Discrete nozzles on the other hand injects powder in beams from each nozzle. The number of active discrete nozzles can vary depending on application.

A dilution area is created with the mix of melted powder and melted substrate as the heat source moves over the substrate. Deposited material is fused with the substrate in the dilution area, in presence of an inert gas. The inert gas is necessary to avoid undesirable oxidisation in the sample.

3 Methodology

In this section, the methods and approaches that have been used are described.

3.1 Literature study

A literature study was conducted in order to gain knowledge in current and established research [25] within the topic of the thesis. The purpose was to continuously be able to identify valuable papers, gaining new and deeper knowledge and understanding [26].

A literature search was formed based on the purpose and aim of the thesis, focusing on Ni-based superalloys in general and Waspaloy in particular. Features and properties pertaining to crack formation, geometrical defects and microstructural grain growth was of particular interest. Research relating to formation of cracks in a wide range of metals in general were included too, as these studies may enlighten with information regarding to effects of defects, and possible mitigation techniques. Furthermore, the type of processing method used in other studies was of interest and was taken into consideration. Studies considering crack formation in the context of DED were important for putting this thesis in a clear comparative research context, where results are possible to compare and justify.

The literature study was performed partly in parallel with the experimental research. This approach was necessary in order to be able to fill knowledge gaps during the practical experiments.

Databases and meta-databases including academic search engines were used in the search process. Topics and specific search patterns were used in Google Scholar, Chalmers Library, University West library, ScienceDirect, Elsevier, CORE, amongst others. Screening was made on physical books, journal articles and proceedings, and limited to written texts. Search strings in the databases was created by a combination of one or more keywords. Keywords of particular interest is presented below.

Keywords: Waspaloy, Additive manufacturing (AM), Repair and maintenance, Superalloys, Crack, Defects, Direct energy deposition (DED), Laser-directed energy deposition (LDED), Nickel-based, Microstructure, Mechanical strength, Laser metal deposition (LMD)

Journals and online sources was screened by reading title and provided summary. If both the title and the abstract was deemed of interest and relevant, the text was downloaded and saved. Saved literature was read thoroughly, and information extracted if it was found applicable to the thesis.

3.2 Experiment

In order to gain insight in the manufacture of components in Waspaloy using L-DED-P, the manufacturing process of samples, built for my analysis, was observed. An understanding to the practical process in terms of how it works in reality was deemed important in order to appreciate the different factors influencing on the built result and to better understand the overall process, including preparation and build time.

Analysis of the produced samples are the main topic of the thesis, and thus, is of primary importance. However, the analysis is partly destructive and a thorough plan was needed to not waste material.

3.2.1 Analysis

A general analysis included the following steps:

1. Rough cutting of samples into dimensions suitable for precision cutting.
2. Precision cutting of samples into pieces of suitable dimensions in preparation for hot mounting.
3. Rough grinding to even the surface of mounted surface.
4. Grinding with gradually finer grain size and higher grit.
5. Polishing with gradually finer polishing discs.
6. Etching of surface with oxalic acid ($H_2C_2O_4$) electrolyte
7. Analysis of microstructural surface using optical microscopy
8. Hardness testing

The steps can be divided into sections of cutting, grinding/polishing, etching, microscopy analysis, and hardness testing.

3.2.2 Sample plates for analysis

Steel substrate plates with built samples was prepared beforehand. The plates were a total of seven, and consisted of eleven different process setups (see Appendix A for process parameters) where each setup included four different layer heights. The number of layers were 1, 3, 5 and 15 for each setup. In addition, three additional builds using midpoint values was made.

The samples were built on substrate plates made of stainless steel 347 with the dimensions 150 mm × 60 mm × 3 mm. The samples were built along the width of a plate, with start 5 mm from an edge, and end 3 mm from the opposing edge, see Figure 2a. Rough measurements of deposited sample was made with a vernier caliper from Mitutoyo with a tolerance of ± 0.05 mm. The length of the build samples measured 52 mm, and the width 2.6 mm.

All of the substrate plates were exposed to the heat from the laser during manufacturing of the samples. The heat affected the plates such that thermal expansion and contraction occurred, which resulted in the substrates bending. In trying to mitigate the thermal effect, and minimise the bending, each short end of the substrates was tack-welded onto a common 20 mm thick bottom

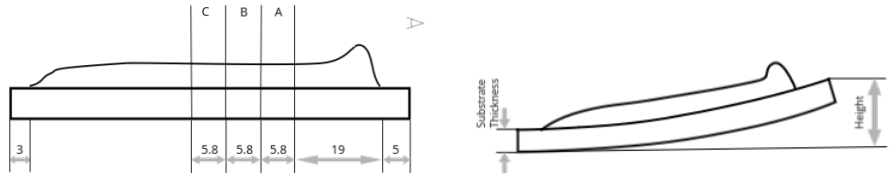

(a) *Sketch of substrate and sample showing where cuts are made for collecting three cross-section samples A, B, and C. The perspective is shown with the eye indicating which surface of the cut that is analysed.*

(b) *Sketch showing deviation from flatness of samples after build. The deviation is calculated by subtracting substrate thickness from the measured height. All dimensions are shown in millimeters.*

Figure 2: *Sketches of cut geometry and flatness deviation.*

Table 4: *Deviation from flatness of samples cut in groups of three from plates originally fitting nine. Deviation is measured by holding one side of the sample flat against a surface and measuring the height of the opposing end. From the measurement is the deviation calculated by subtracting the thickness of the plate. No account is taken for the curvation of the plate, and thus the values obtained are an approximation, and higher than if a more stringent method would have been used.*

Samples	Deviation [mm]	Average deviation [mm]
1	2.7	
2	3.0	2.9
3	3.5	
4	3.8	
5	3.4	3.1
6	2.1	
7	3.0	2.8
8	2.7	
9	3.5	
10	2.9	3.6
11	4.5	

plate. This maneuver however did not fully succeed in keeping the plates flat. In Table 4 the deviation is presented. Before measurement, a rough cutting has been made and cut the plates in smaller sizes, dividing all samples in groups of three, save for one which is grouped in two. The bending is measured by pushing one side of the samples flat onto a plane surface, and measuring the distance between the top of the plate and the flat surface on which it lies on, see Figure 2b. Samples built with fifteen layers have deviations presented separately in Table 5, separated in groups of two or three samples.

3.2.3 Rough abrasive cutting

Before analysing samples, the plates have to be cut into smaller and manageable pieces. A first cutting was done with an abrasive cutting machine of type *Buehler Abrasimet 2*. A 10 in (254mm) in diameter, 1.3 mm thick abrasive cutting blade *Buehler 12-4205-010* suitable for superalloys and general steel was used with the machine.

Table 5: *Deviation from flatness for plate built with fifteen layer samples cut in sets. The deviation is measured normal to a plane, up to the maximum height of the substrate. The thickness of the plate is subtracted, but no consideration is taken to the curvature of the sample set.*

Samples	Deviation of flatness [mm]	Average plate deviation [mm]
1, 5, 9	16.7	15.8
2, 6, 10	17.0	
3, 7, 11	17.1	
4, 8	12.4	

Table 6: *Width of rough cut samples. The width of the sample corresponds to the length the sample will have after mounting.*

Sample	Width [mm]
1	27.00
2	27.60
3	26.10
4	26.70
5	27.05
6	27.00
7	26.80
8	27.15
9	27.75
10	26.30
11	26.35
12	29.30
13	27.75
14	28.10
15	19.80

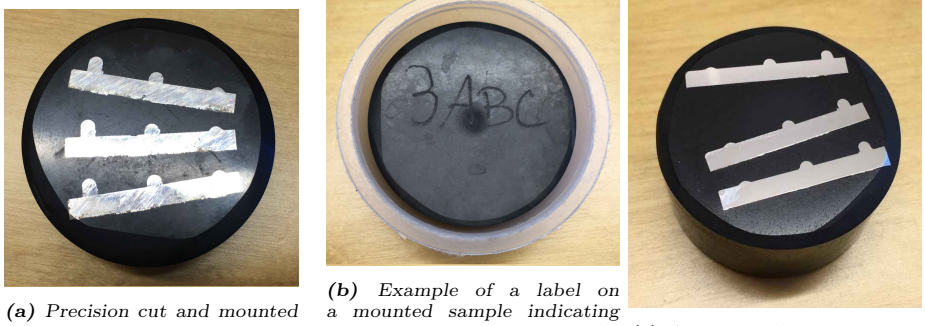

(a) *Precision cut and mounted samples, each representing a specific cut surface.*

(b) *Example of a label on a mounted sample indicating what process setup was used for building the samples.*

(c) *A sample after the process of grinding and polishing.*

Figure 3: *A mounted set of samples in unpolished and a polished state. Within a certain the mount, the samples all use the same process parameters, but represent builds with 1, 3 and 5 layers respectively.*

The substrates were cut into pieces of suitable width for further finer cutting. Pieces from the rough cutting had widths according to Table 6. Length of each piece after the first cutting was the width of the original plate, which was 60 mm.

3.2.4 Precision cutting

The purpose of rough cutting was to group samples and to cut the original metal plate substrate into more convenient and manageable pieces. In preparation for precision cutting, the rough cut pieces was marked with the locations of where to precision cut. Each cut piece was measured, and markings were placed at 24 mm, and three times 5.8 mm from the previous marking. The marking at 24 mm is measured from the substrate edge on the side where the L-DED-P process started, see Figure 2a. Each sample was cut such that three sample pieces were attained, each measuring approximately 5 mm in width.

A *Struers Secotom-10* [27] precision cutter was used with a Silicon Carbide (SiC) cut-off wheel of type *Struers 10S20* for soft non-ferrous materials. The cutting wheel had a thickness of 0.8 mm. Parameters in cutting was with a set cutting length of 30 mm to 34 mm, and disc rotation speed of 3000 rpm and a feed of 0.60 mm/s to 0.130 mm/s. The machines' load indicator was monitored and the feed adjusted in order to have a continuous load of less than 30%.

Precision cutting and mounting resulted in three sets of samples mounted in one single mount, see Figure 3. Samples mounted together before polishing is shown in Figure 3a, and the labelling on top of the mount is shown in Figure 3b. All samples were prepared in a similar manner resulting in a set of samples with a rough and uneven surface finish.

3.2.5 Labelling sample pieces

Precision cut pieces were hot mounted with moulding compound in a mount of size 40 mm in diameter. Three pieces of the same sample group were mounted together and labelled with a number corresponding to the manufacturing parameters. The fifteen layer samples were cut with the same measurements, but are labelled differently. The labelling starts with a F-letter prefix (signifying

Table 7: *Discs used with Buehler PowerPro 5000 for grinding and polishing of mounted samples. An additional liquid compound was used in the grinding and polishing steps from, and including, disc with grain size 9μm.*

Name	Grain size
Steel Cameo Disk	58 µm
Steel Cameo Disk	25 µm
Steel Verdu Tex	9 µm
Steel Verdu Fix	3 µm
Steel Chemomet	0.06 µm oxide polishing

15 in the hexadecimal numerical system), and is followed by which samples are present. The three pieces are also labeled with characters A, B, C, where the letter represents how far into the sample the cut was made. Letter A represents a sample cut between 24 mm and 29 mm from the edge of the substrate. Letter B represents a piece cut between 29 mm and 34 mm, and finally letter C represents the piece between cuts 34 mm and 39 mm. The pieces are placed such that the surface for analysis is not repeated. That is, pieces labeled A are analysed on the surface made at 24 mm, pieces labeled B on the surface of a cut at 29 mm, and C-pieces at the 34 mm cut, see Figure 2a.

3.2.6 Grinding and polishing of samples

Mounted samples were ground and polished using an automatic grinding and polishing machine *Buehler PowerPro 5000* using incrementally finer grain size discs. Table 7 describes the discs used, and the corresponding grain size. Setup of the machine set the method of operation to *Buehler Method 16*. The method is used for nickel based alloys superalloys and is a step procedure consisting of four steps. Steps two through four is used with liquid compound automatically dispensed by an automatic dispensing unit. Step number one is repeated once, and is run for both the Cameo Disks with grain sizes 58 µm and 25 µm. Water rinsing is activated for step one, but inactive for steps two, three and four, where the liquid dispensing is used.

According to the method, a force of 30 N is put on the individual samples during grinding and polishing. The disc speed is 240 rpm for the first step and 120 rpm for the remaining ones, and the head speed is 60 rpm throughout. The first three steps have a compliant head direction, which spins in the same direction as the disc. The last step has a opposing direction for the head and the disc. Rinsing water is activated on the disc for the final 40 s of the final procedure step.

All samples and the head was thoroughly cleaned in between procedure steps using soap and water. An additional cleaning was performed after steps three and four, utilising an ultrasonic cleaner where the samples were fully submerged in ethanol. The cleaning time in the ultrasonic cleaner was approximately 20 s for each set of samples. The final polishing induced a cleaning procedure in three steps, with ultrasonic cleaning, followed by washing with soap and water, followed by rinsing with ethanol. Ethanol from the rinsing was dried with a heat gun with the sample put at a steep angle.

Cleaned samples was placed in individual plastic containers for scratch-free storage and portability.

An indicative result of a grinding and polishing process of the samples are shown in the example of sample 3, see Figure 3c. The surface of the samples were polished to a mirror-like finish, removing unevenness, scratches, and contaminating residue.

3.2.7 Light Optical Microscopy

An optical microscope was used for investigating the surface area of the samples, with magnification of 12.5x. The low magnification was used to get an overview of a sample, looking at it in full view. The procedure was successful in quickly identifying defects such as larger pores and cracks, as well as geometrical properties. A microscope of type *Olympus BX60M* with an attached digital camera *Axiocam 305 color* was used in the analysis. Magnification in the eye piece was fixed at 10x, with a variation of optical lenses for magnifications ranging from 1.25x to 100x. Each sample was placed in the microscope such that the substrate was lined up horizontally, with the Waspaloy build towards the positive vertical axis. Each sample was analysed and photographed with the camera using the software *ZEN Core v.3.3.92.00000*.

Analysing the images, including the detection and size-measurements of pores and defects, was performed semiautomatically with the use of *Fiji (ImageJ) 1.54f*. Before the analysis however, the images were cropped and reduced in size by removing extraneous image material showing the substrate and mount. The build and the heat-affected zone with the substrate was left after cropping. *Gwenview 22.12.3* was used for this preanalysis action.

ImageJ was used to semitautomatically identify and measure potential defects. The analysis was performed by calibrating the scale used internally within the software. This calibration was performed by drawing a straight line with start and end points placed on a known length, and inserting this length into ImageJ as the real length of the drawn line. Geometrical measurements were taken on samples, where the height, penetration depth, and width was recorded. All measurements use the top of the substrate as a common reference. The height is measured vertically from the substrate to the highest point of the continuous mass of the built sample. Powder particles not fully fused with the material were ignored in the measurements. The width was measured horizontally across the sample, yet again ignoring parts and/or particles exhibiting low level of material fusion. Penetration depth was measured vertically into the substrate, measuring the depth of the fusion zone. An illustration showing the where the measurements are taken is showed in Figure 4

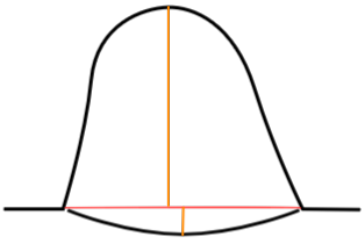

Figure 4: *Illustration of where the measurement were taken, showing the width in red and the vertical distances representing the height and penetration depth into the fusion zone in orange. Note that the straight horizontal black lines represent the top of the substrate and act as a reference for all measurements.*

Pores and defects were automatically measured with ImageJ using the function of “Analyze Particles”. Threshold limits were set using the “Threshold”

function to ensure that defects were highlighted, whilst the rest of the build was outside the threshold limit. Limits were applied to the image, rendering an image with full contrast, where the pores were coloured white and the surrounding material coloured in black. Defects were automatically found and analysed, and the results saved included the area and feret diameters for each identified defect.

3.2.8 Hardness testing

Samples were hardness tested on a *Shimadzu HMV-2T* with an attached camera of model *Sentech STC-TB33USB-AT-F* using HV0.5 Vickers hardness with 12 s dwell time. The hardness test was performed on samples which had a fully exposed cross sectional area without edge damages. Hardness indents were placed with an initial offset 0.1 mm from the top of the build, and a following distance of 0.2 mm between each consecutive indent throughout the middle of the build, from the top and downwards into the fusion zone of the substrate plate. Testing was canceled at the point where the next indentation would have occurred fully in the substrate.

3.2.9 Etching

For enhancing contrast in the sample, electroetching was applied. A DC power suppply *PeakTech 6080* provided voltage and current. The voltage was set to 3.0 V and the current set to approximately 25% of max. Oxalic acid with a concentration of 10 wt% was used as electrolyte and put on the samples. The anode and was connected physically with the sample substrate, and the cathode hovering over the sample, but touching the electrolyte. Active etching time with a full circuit was no longer than 1 s for each sample.

4 Results

This section presents analysis results, both qualitative and quantitative.

4.1 Analysis with light optical microscopy: A visual assessment

Within the analysis with the optical microscopy, the structure and geometrical accuracy of the samples was investigated. The analysis primarily focused on photos showing an overview over whole samples. An example of this is shown in Figure 5a.

A qualitative assessment was made based upon visual inspection of the samples. Each sample was analysed in the three different cut areas, A, B, and C, and a summarising judgement is provided below for all layer heights combined. The three surface areas serve the purpose of finding a fair representation for the sample as a whole, irregardless of layer height. Below is a review of the samples after this assessment, with a descriptive wording characterising defect sizes in small, medium, large, and the number of defects in terms of few, couple and numerous. Sizes are primarily to be considered for pores, where the sizes are corresponding as follows: Small = 5 µm, medium = 10 µm to 15 µm, and large 20 µm or bigger. Quantification of the number of defects are mapped in the follow manner: Few = 1 to 4, multiple 5 to 8, numerous 9 and more. Lack

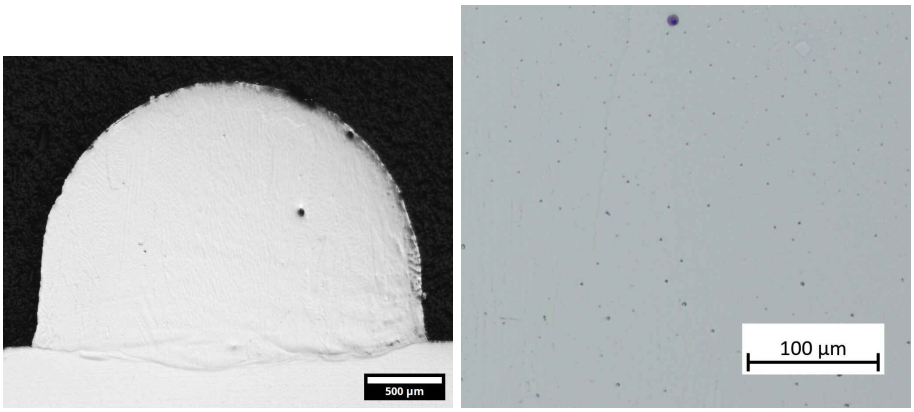

(a) *Overview image of sample 1, cross section at cut "A", built with 5 layers.*

(b) *Cross section at cut "B", with 50x magnification*

Figure 5: *Detail and overview image of sample 1.*

of fusion occur in some samples, and are specifically mentioned if they do. If there is no mentioning of lack of fusion, the description is only describing the properties of the probable pores.

Sample 1 Multiple pores with common defect sizes in the range of 5 µm to 10 µm, with a preference towards the lower range. Seems to be a high density of smaller pores uniformly distributed within samples in sizes approximating 1um. The fifteen layer build is in line, and exhibits a few pores of medium size.

Sample 2 Few defects in general, but the sample has examples of both small and large pores, in varying all sizes from small to large. Lack of fusion defects are observed, as well as unmelted particles on the outer shell of the sample. The build has no noticeable penetration with the substrate, with no recorded fusion zone depth. Voids in the shell are commonplace, where the powder has not fully fused with the deposited material. The fifteen layer build exhibits numerous scattered small pores and lack of fusion cracks.

Sample 3 Overall clean samples with few pores of medium to large size, with consistent results throughout all layer heights.

Sample 4 Numerous defects in sizes up to 5 µm, and a few medium and large pores respectively. A few possible lack of fusion, and unmelted powder particles on the outer edge. Especially in the fifteen layer build the defects are predispositioned towards lower 2/3 of the build, whilst the top 1/3 is rather free of defects.

Sample 5 Populated with evenly distributed smaller defects and small pores, with few medium-large size pores.

Sample 6 Numerous smaller defects and specifically lack of fusion with lengths of 15 µm to 20 µm. Few pores medium sized pores, and a single pore of 30um. Notable lack of of fusion to the substrate with cracks emerging

between the substrate and the build. In addition to the internal defects, there are also unfused particles on the outer edge of the build.

Sample 7 Deep material penetration within the substrate, and a build that shows only few signs of defects. There are few small defects, and a lack of fusion crack with a length of 15 µm. The fifteen layer build shows numerous pores of medium size and smaller, and a lack of fusion.

Sample 8 Samples with three and five layers exhibit numerous pores, mainly in medium size, but a few larger pores, with a single one measuring approximately 50 µm. A few possible lack of fusion measuring 30 µm. In the fifteen layer build only few defects are found, shown as medium sized pores.

M1, M2, M3 Few defects, and smaller in size for the builds with layer heights of 1 to 5. Overall clean samples, with few signs of smaller pores in sizes of 5 µm. Characteristic for all midpoint samples are a consistent result showing similar number of and severity of defects. Overall impression of the fifteen layer midpoint builds is that the pores have increased in quantity. Multiple large and medium sized pores are found, in addition to numerous small ones.

4.1.1 Observations on etched samples

Etched samples show the grain structures and the growth of the dendrites. For all samples, with possible exception for single layer samples, there is a growth of columnar structures in the vertical axis. In multiple layer samples a band structure is observed after etching, the bands appears in brighter and darker segments in a wave-pattern, corresponding to the different layers.

4.1.2 Qualitative and visual notes on sample geometry

Sample shapes follow a bell shape curve, with a varying degree of width and height. Typical appearance are smooth, continuous curves outlining the surface edge of the samples. Single layers samples tends to have a smooth transition between the substrate and the build in an obtuse angle in the range of 135° to 155°. The angle between the build and the substrate decreases with more layers, converging towards orthogonality. At the top of build samples, the shape is half-circular.

Geometrical properties in the fifteen layer builds show samples with abnormal behaviour, that is, the samples are diverging from mean shape. Sample 5 is wider at the base than in the top, and there is an angle that suggests that the total width at the base is wider than in the top section. Sample 6 shows varying widths throughout the build. The sides of the samples exhibit wave-like behaviour, with the width expanding and contracting. The difference between the maximum and minimum width in the sample is in the range of 200 µm to 300 µm. Sample 2 is showing a leaning behaviour, where the layers are built such that the structure is experiencing a leaning angle of $4 \pm 2°$. Sample 7 has a low height, and the shape is noticeably round.

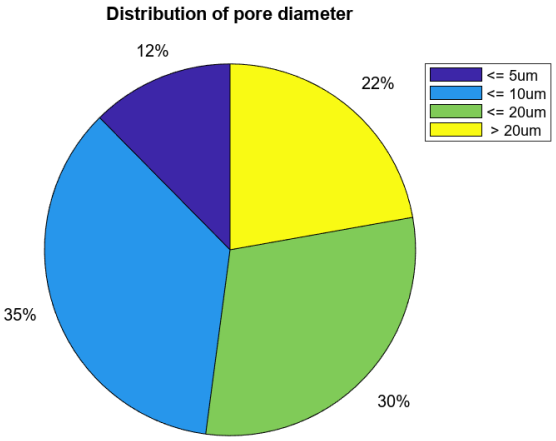

(a) *Distribution of the feret diameter of pores from sample 1. The distribution is representative for all samples.*

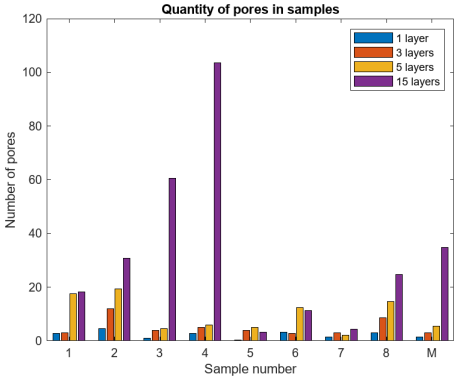

(b) *The quantity of pores for each build, where the data is averaged over three surfaces.*

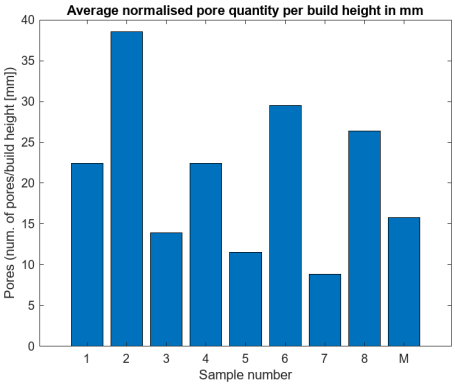

(c) *Normalised pore distribution per millimeter build height. Midpoint values M1, M2 and M3 have been averaged and the result is shown as sample M.*

Figure 6: *Properties of pore defects in samples.*

4.2 Postprocessing and analysis with ImageJ

An analysis on all samples was performed with ImageJ, where defects were identified and measured automatically by the software. After filtering the data for pores, there was a clear pattern for all samples in regards to the size of pores. In the following, defects and pores are used interchangeably, but both refers to pores and other defects with feret diameters within a set filter threshold. The filter threshold dictated that the maximum feret diameter and the minimum feret diameter must not differ more than 10 µm. Samples M1, M2, and M3 are averaged, and the result is called *sample M*.

A distribution of the feret diameter of the pores are shown in Figure 6a. All samples share approximately the same distribution, with only slight variation. The overall results that is consistent throughout is a distribution of pore sizes as follows: 20% larger or equal to 20 µm, 30% 10 µm to 20 µm, 30% 5 µm to 10 µm, and remaining 10% smaller than 5 µm.

There is no observed preference in the locations of the pores. The occurrences and size of the pores are stochastically distributed throughout each sample. In builds with low build height, the quantity of pores are generally few, and as the build height increases with the number of built layers, the amount of defects also increase. The increase of the amount of pores is for most samples substantial between the five and fifteen layer builds. Pore quantity in samples is shown in Figure 6b.

Samples 5, 6, 7 show few defects overall, and especially noteworthy is that the fifteen layers does not exhibit a significant increase in defects compared to the builds with fewer layers. In sample 6 the most defects are found in the five layer builds, with a few more than in the fifteen layer build. The sample exhibit a sudden increase in pores in builds with five and fifteen layers in contrast to the single and three layers. The fewest defects are found in sample 7, and the fifteen layer builds has slightly more pores than the five layer builds. Sample 5 shows low degree of defects for all layers, where both the single layer and the fifteen layer builds have the least amount of defects.

Sample 4 is by far the sample with most defects, but only for the fifteen layer builds. The sample presents however few defects for builds with one, three and five layers. For these builds, the amount of defects are corresponding to the quantity shown in samples 3, 5, 7. In sample 5 the number of defects is not increasing with the fifteen layer build. There is however a major increase in the quantity of defects for samples 3 and M between the five and fifteen layer builds.

In further analysis, the defect quantities have been normalised with regards to each samples build height. The normalised values have been averaged for all build heights, see Figure 6c. Each bar represents the average number of expected pores per millimeter in build height. Sample 2 is the sample most prone to experience defects at 38.5 pores/mm. Sample 7 indicates the least degree of defects with a rate below 8.8 pores/mm, with sample 5 and 3 following at 11.5 and 13.9 pores/mm respectively.

4.3 Geometrical properties and accuracy

Sample build heights are presented in Figure 7a. Samples three and four have a maximum build height at 7559 µm and 7234 µm. Both samples represent the

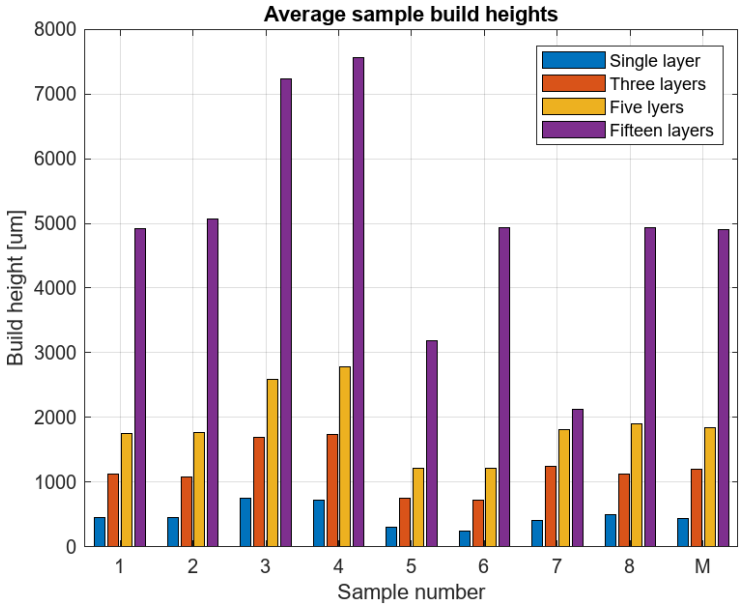

(a) *Build height of samples.*

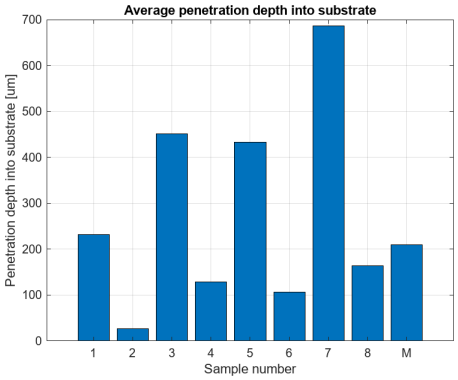

(b) *Average penetration depth into the substrate.*

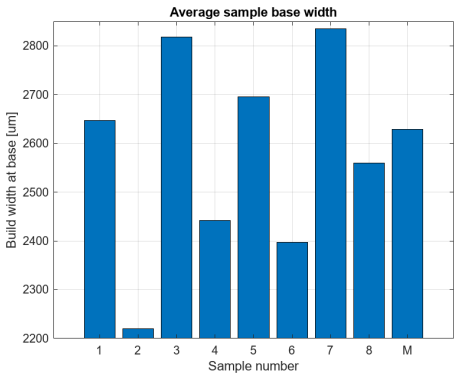

(c) *Base width of the samples measured from the top surface of the substrate.*

Figure 7: *Geometrical properties of samples showing build height, base width and penetration depth.*

fastest build rate irregardless of the number of built layers. Four samples are 2000 µm shorter than the top results, but all measures approximately 5000 µm at the fifteen layer builds, namely the samples are 1, 2, 6, 8, and M. All these samples have similar build development, as follows: A single layer height measures 200 µm to 400 µm, a three layer height approximately 700 µm to 1200 µm, and a five layer height 1200 µm to 1800 µm. The sample with the least accumulated height is sample 7, which at the fifteen layer build measures slightly more than 2133 µm.

Maximum penetration depths are presented in Figure 7b. It can be seen that sample 7 has the deepest penetration which measures 687 µm, and sample 2 the least with a depth of 27 µm. Sample 4 and 6 has an average depth of the fusion zone at 129 µm and 106 µm respectively. The three samples 1, 8, and M measure 232 µm, 164 µm and 210 µm. Sample 3 and 5 has a fusion zone depth measuring 451 µm, and 432 µm.

Widths measured straight across the base of the samples are shown in Figure 7c. It can be seen in the figure that samples 3 and 7 are widest with a width at 2818 µm and 2834 µm. Sample 2 is at the other end, with a width of 2220 µm. Samples 4 and 6 measures 2441 µm and 2396 µm. The four samples 1, 5, 8, and M all measure in the range 2500 µm to 2700 µm, with widths 2647 µm, 2695 µm, 2559 µm, and 2628 µm.

4.4 Hardness testing

Hardness testing in the three layer samples show a mean hardness of 240 HV, with peak hardness for sample 1 which exhibited a hardness of 285 HV at the distance 200 µm from the substrate. Sample 2 consistently reports hardness of approximately 255 HV throughout with the exception for an indent bordering to the substrate surface. Sample 7 shows low hardness at 210 HV and below.

In the five layer case, the hardness of the samples range between 230 HV to 280 HV. Sample M exhibits a peak hardness at around 280 HV, but cannot uphold the hardness throughout, and drops to 250 HV to 260 HV within 400 µm of the maximum. The maxima are located at different locations for each of the midpoint samples. One of the samples have a maxima at the top of the sample, another has a local maxima 400 µm below, and the third sample has the maxima placed in the near middle, halfway between the substrate and the top edge. Sample 2 performs consistently as in the three layer case, with a hardness of 260 HV to 270 HV. Sample 3 has a declining hardness, with a maxima of 270 HV and a minima of 240 HV. Sample 5 shows a hardness curve in the shape of a convex parabola, with a maxima of almost 240 HV at 400 µm from the substrate.

Fifteen layer builds report the highest overall hardness for all samples. Sample 5 has hardness ranging from 250 HV to 302 HV, with a plateau at 270 HV to 280 HV. Sample 2 shows a maximum hardness of 310 HV at the floor of the sample, by the substrate, with a decreasing hardness as the indents tends towards the top. The minima of 250 HV is found in an isolated point at 3000 µm, but the overall low hardness of the sample is averaging 270 HV to 280 HV. Sample 3 peaks with 325 HV at 2000 µm, and has decreasing hardness values on both sides, both higher up in the sample, as well as below. The plateau of high hardness (at and above 300 HV) ranges from 1000 µm to 3200 µm. From the peak values of 300 HV and above, the hardness decreases to 260 HV to 270 HV

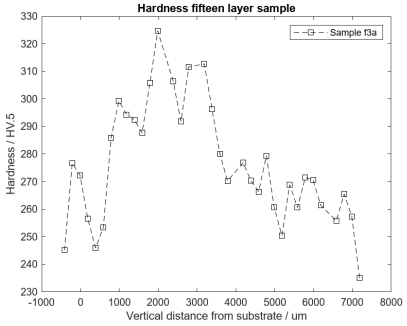

(a) *Hardness in the fifteen layer build of sample 3.*

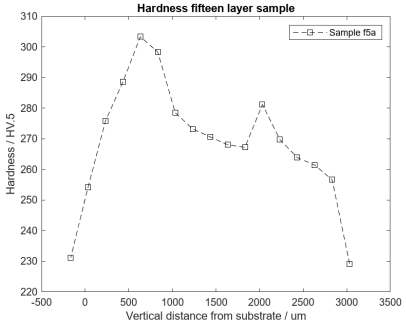

(b) *Hardness in the fifteen layer build of sample 5.*

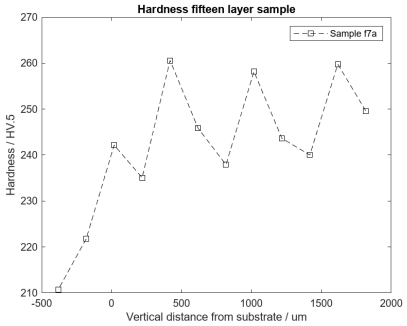

(c) *Hardness in the fifteen layer build of sample 7.*

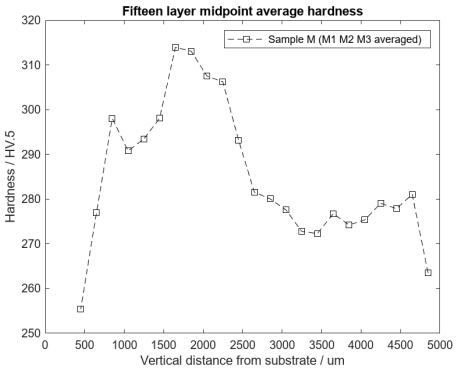

(d) *Hardness in the fifteen layer build of sample M.*

Figure 8: *Hardness in three samples showing characteristic differences.*

within 400 µm. Sample 4 shows similar hardness response as sample 3. Sample 6 reaches 350 HV for an indent close to the substrate. Except for the single indent, a hardness of 290 HV is evenly distributed from 1000 µm and higher in the sample. Below the 1000 µm mark, the hardness is gradually increasing towards the peak value.

In sample 8, the hardness is divided in two areas. Between 400 µm to 2600 µm, the hardness is at and above 280 HV, gradually increasing towards a maximum hardness value of above 320 HV at 2600 µm. From 2800 µm and onwards, the hardness was 260 HV to 270 HV. The same phenomena with two distinct levels of hardness is evident in sample M too, with the segments having a hardness of 270 HV and 310 HV. Sample 7 records the lowest hardness of fifteen layer samples, with hardness values ranging between 240 HV to 260 HV, through the sample.

5 Discussion

The results are spread wide, and there is a significant variation between the results of the individual samples. There are differences in the geometrical properties, as well as in the hardness and the amount and quality of pores, and defects.

5.1 A note on single layer builds

Single layer builds in general have a small surface area to analyse, which hinders an effective analysis in all areas save for the geometrical measurements. The hardness testing results are few, and the indentation point in the material is potentially within the fusion zone where the Waspaloy and steel substrate was mixed. Only a few hardness measurements could be taken per sample due to the low height of the builds. All single layer samples show a low relative hardness compared to builds with more layers. One can speculate if this low hardness is due to the build material fusing and mixing with the substrate, or if it is an effect of the manufacturing process and handling of the Waspaloy in the powder form. It is noticeable however, that the dendrites and grains have not formed columnar structures in the vertical axis. However, a columnar structure may as well have been formed in a horizontal axis, in the direction along the axis of the laser scanning.

The amount of pores in the single layers builds are few, but it is again an effect due to the low build height. There simply is not much area that can be affected by defects, and although there is only a single layer, there is a difference in layer height depending on the processing parameters. Samples 5 and 6 present especially low layer height, whilst sample 3, and 4 have a high layer build even for a single layer. Due to the low height overall, the proportion of amount of pores are greatly affected by the number of pores found here. Even for a small amount of pores, the concentration is volatile and prone to fluctuation between samples, even if the quantitative difference is small.

5.2 A note on 3, 5, and 15 layer builds

Increasing the number of layers affects the samples properties in all measured matters, except for the base width, and the penetration depth. The hardness testing results show a general increase in hardness throughout the samples. Measuring on the three layer samples give a slight, but distinct overall hardness increase compared to the single layer results. The height is increased, and all samples without exception experience an increase in height. The total build height increases by a factor of approximately 2 or 3, depending on the sample.

Not until the fifteen layer builds does the pore count accumulate such that there is significant differences between the samples. Especially sample 3 and 4 stands out with a pore quantity more than double and three times as the rest of the samples. Both these samples too share the same high build height, reaching the highest. The differences between the two samples are the power input, which was high in the case of sample 3, and low for sample 4. The scanning speed and the feed rate was kept at low and high respectively.

5.3 On sample 3 and 4

Sample 3 and 4 share both processing parameters and characteristic results. Whilst sample 4 has slightly higher build height, the fusion zone is deeper, and the base width wider in sample 3. Sample 3 has a stronger bond to the substrate due to the deeper penetration and the wider width of the fusion zone at the base. Both of the samples however, show a high degree of defects, and the quantity of identified pores in either sample is considerably more than in other samples. The normalised pore quantity per millimeter build height shows that the build height does in some regard counter the amount of pores. That is, the amount of pores in relation to the build height is on a medium to low level, compared to other samples. Especially sample 3 is promising in this area, where the sample performs in the top three with the least amount of defects per millimeter.

The hardness of sample 3 as shown in Figure 8d indicates two levels of hardness, with a lower degree of hardness at the top of the sample. The material shows higher hardness between 2000 µm to 3000 µm from the substrate. This height is at one third of the total sample height, and the material has, during the manufacturing of the top layers, continuously deposited heat into the sample and previously built layers. The continuous heat input may have initiated a hardening process. During the hardness testing, the effect of the involuntary hardening shows up with the hardness surpassing 300 HV.

5.4 On sample 2 and 6

In the same manner as sample 4, both sample 2 and sample 6 too has a low penetration depth, resulting in a weak fusion bond with the substrate. The base width of sample 2 is the most narrow of all samples, and although sample 6 has a wider stance, it is the second most narrow. Both of these samples therefore are characterised with a weak and narrow bonding to the substrate, with almost nonexistent penetration depth, especially in sample 2. Whether a weak or strong substrate bonding, it has however not inflicted negatively on the build height performance. The build rate is on par with samples 1, 8 and M, with a fifteen layer height of 5000 µm.

Comparing between the two samples, the defects are plentiful for sample 2, but the identified defects are quite few in sample 6. The normalised amount of defects show that sample 2 is by margin the sample most prone to defects. Sample 6 is the second from the top, and positions itself as the second worst. In the qualitative analysis, it was observed that both samples suffer from pores and lack of fusion. It was noted that sample 6 especially suffered from small pores and lack of fusion. Sample 2 was mainly affected by pores in varying sizes, but with fewer other defects noted. Both samples show unmelted and unfused material in the shell of the material. The material fusion seems to be lacking, and the powder was not fully melted and fused with previous layers.

The process parameters for the samples vary only in feed rate. In both samples 2 and 6, the manufacturing used a low laser power of 1150 W, and a high scanning speed of 25 mm/s. The powder feed was high (16 g/min) for sample 2, and low (10 g/min) for sample 6. The low laser power and the high scanning speed indicates that the power input on each point in the material will be low and quickly distributed. Both sample 2 and sample 6 show high hardness close to the substrate, with hardness values reaching 350 HV in sample 6. The samples share the common treat of a decreasing hardness with distance from the substrate. Both samples thus experience hardening in the lower sections of the samples, which is incident to the continuous heat low input. The heat input does not fully remelt the material, and as discussed, the power is not high enough to sufficiently melt and fuse powder particles to the underlying material. Still with pores and lack of fusion, the simultaneous building and hardening of lower layers renders a partially hardened material infused with defects.

5.5 On sample 1, 8 and M

Samples 1, 8 and M all have similar penetration depth, base widths and build heights. The penetration depth is at 200 µm, and the base width at 2600 µm, with a build height as mentioned above. Concerning the fifteen layer builds, the most pores are identified in sample M, with sample 8 and 1 presenting slightly fewer defects. However, the total normalised pore distribution instead shows a different order, where the lowest degree of pores per build height is found in averaged middle point samples M, followed by 1, and 8. A reason for the discrepancy between the quantity of pores and the normalised results lies in the amount of pores found in the builds with layers 1, 3, and 5. Although sample M shows a high quantity of pores in the fifteen layer builds, this is not the case for the lower build levels. The contrast is stark, and indicates a reduced tendency to form pores and defects in lower build heights. Sample 8 reveals more pores as the build height increases, and in sample 1, the amount of pores in layers 1, 3 are few, while the five layer build shows like quantity to the fifteen layers. Averaged over all build heights, sample M shows the best results, with lowest pore distribution of the set.

Defects in the midpoint samples increase in both quantity and size in the fifteen layer build, which was noted in the qualitative analysis. Defects in sample 1 seems to be more frequent in the smaller sizes, with a high frequency and even distribution of tiny pores, with larger pores as infrequent, which is a contrast to sample 8 which shows a possible lack of fusion, in addition to pores of predominantly medium size. Though lack of fusion cracks are present in the samples, the dominating type of defect is the pore, which occurs in medium and

smaller sizes. No large pores are evident in the analysed samples, but rather the analysis shows an incline towards well distributed pores. In the broader picture, given the set of these three samples, the quantity and severity of defects are few and seemingly mild.

Sample 1 was built with high laser power, high scanning speed and high powder feed, sample 8 was built with the opposite in all parameters, using low power, low speed and low feed. The midpoint samples was built with the mid-values in all parameters. The results show that the process parameters being consistently in the same class (low, medium, or high) gives a consistent result, whichever set of parameters was used. It can be noted, though, that sample 8 did show excessive signs of longer lack of fusion formations, and occasionally pores the size of a powder particle. These defects may have occurred due to the low laser power. Lower heat input thus seemingly promotes the generation of larger pores, while a higher heat input, scanning speed and feed, promotes more but smaller pores, and a less likelihood to find lack of fusion. The midpoint samples however seem to give the most clean samples, and as such provides a midway in where the large pores are absent, and the small pores only occur in low quantities. Even the lack of fusion cracks seemingly are absent in the samples, giving the midpoint samples an advantage in defect performance, still upholding the same geometrical properties as the other samples.

5.6 On sample 5 and 7

Sample 5 and 7 are low performing in the build height area. The fifteen layer builds measure 3000 µm and 2000 µm respectively. Either sample have a different height development. Sample 7 have a substantial build height performance between the single layer and layer five, but only minuscule increase in the fifteen layer build. By contrast, sample 5 shows meager build height development up to layer five, but more than doubles the height in the fifteen layer case compared to the five layer. Thus, there is a significant difference in how the samples behave in building layers when the number of layers increase. The penetration depth is deep for both samples, and up to 700 µm for sample 7. The base width is wide, with sample 7 being the widest of all analysed samples. Sample 5 measures almost 2700 µm which is third widest.

On a positive note, the samples have very few defects, they are both far better in this regard than other samples. The quantitative amount of pores is low, with only a few identified defects irregardless of the number of built layers. Both sample 5 and 7 present near perfect cross-section surfaces, smooth and with only minor defects. These samples also have the lowest normalised pore distribution, securing their position as the samples least prone to defects.

The hardness of sample 7 is increasing ever so slightly towards the top of the sample, with a distinct reduction in hardness as the indents are placed at the level of the substrate, and into the fusion zone. In the built sample an average hardness of 250 HV is found. Sample 5 shows a peak 500 µm from the base level, with reduced hardness towards the top of the sample. The peak shows a hardness of slightly more than 300 HV, but the average hardness for the rest of the sample lies approximately at 260 HV. Neither sample 7 or 5 is therefore as hard as the partially hardened samples, but the peak of sample 5 indicates that an involuntary hardening still has been engaged in this specific segment of the sample. Sample 7 however shows no indication of hardening, as the hardness

does not show hardness peaks.

5.7 Conclusion

All tested samples have their own characteristic properties. Whether the geometrical properties, or the quantity and quality of the defects, each sample present individual properties. Some samples show excellent build rate, others lack the height, but presents better performance on the surfaces with a low degree of defects. On the topic of defects, it is only pores that have been automatically identified and measured with ImageJ, and thus have been quantified. Other defects, such as lack of fusion, are solely discussed qualitatively.

5.7.1 An optimal sample

Finding the optimal sample in the provided set of sample builds has been part of the goal for this thesis. The best suited sample for achieving a rapid build rate, achieving tall builds and efficient use of infused powder material with a moderate proportion of defects is sample 3. This sample achieves a build height of more than 7000 µm in the fifteen layer build, and gives a highly efficient use of the powder in building fewer layers too. Irregardless the number of built layers, this sample performs well, achieving a tall build with what material is provided. Although the number of defects is quite substantial in the case of pure quantity, the normalised proportion of defects in relation to the build height is low. The hardness for the sample is showing signs of partial hardening occurring in the material as subsequent material layers are built. The hardening phenomena is observed, and might be unwanted in the as-built product, but the hardness results show that no single sample have a flat hardness curve. There are variations in the hardness, and this might be associated with the build process.

5.7.2 Influence of process parameters on build quality

A primary research question for the thesis was to investigate how the choice of process parameters influence the final result in the as-built samples. The question finds its answer in the previous discussion, partly in the optimal choice, partly in the samples that were not considered well-performing – samples where the defects were prominent and the geometrical accuracy poor. Considering sample 3, as the optimal choice of parameters, and sample 2, for a worse choice, it is evident that low power combined with high scanning speed promotes defects. Sample 3 was built with high laser power, low scanning speed and high powder feed, which have showed promising results. By contrast, sample 2 was built with low laser power, high scanning speed and high feed rate, which rendered build scattered with defects. Moreover, sample 5 which in contrast to sample 3 used low powder feed showed weak performance, with a low build height for the fifteen layer sample, which was barely taller than the five layer build of sample 3. The feed rate is therefore an essential component for achieving build height. Sample 4 was much like sample 3, but used a low laser power. This sample provided excellent geometrical properties, but the defects were more than for sample 3. Due to the lower power, the defects may have occurred due to the lack of power, not being able to fully melt and fuse the powder particles.

The scanning speed is the factor that influences how much power that is put into the material. The laser power is a factor that must be in coalition with the scanning speed to achieve an appropriate amount of power in the material, without overheating or remelting the previous layers, and still exercising a balancing act of creating a good fusion with the material.

In summary, the results show that the process parameters of laser power and scanning speed mainly influence on the quality of the build, providing the power and heat input to the material necessary for inhibiting the formation of pores, cracks and lack of fusion. The powder feed on the other hand mainly affects the build rate. Provided a high flow of powder, and given the appropriate scanning speed and laser power, the build rate is dependent on the powder flow. Decreased powder flow lowers the build rate, and an increase in powder flow by contrast increases the rate.

5.8 Further work

The analysis of the work has only been performed with a LOM, and is limited by the capabilities of the microscope. Due to the limitations of the apparatus, the analysis has been performed mainly on the surface area of the samples by visual inspection through the microscope and by analysing photographed microscopy images of unetched samples in ImageJ. The analysis of the surface has not considered the composition of the material, or made particular analysis within the grain structure. Further work can be performed to analyse samples more thoroughly. Ideas on further work follows in the bullet point list below.

- Investigate how the bending of the substrate plates affect the build quality of the samples. In the performed analysis, the substrate plate on which the samples were built was bent during the build of the samples. The thesis has noted a deviation from flatness, but has neither addressed nor considered the effect that this has had on the samples.
- Perform an experiment on the effect of cooling of the samples, and how dwell times affect the geometrical accuracy and the hardness of samples. In the fifteen layer builds it was noted that samples experienced a partial hardening, with hardness values at or above 300 HV not uncommon. Partial age hardening during build is involuntary and uncontrolled, which makes the material and build unreliable with uncertain properties. An investigation and analysis on how the heat from the laser source affects the material and the hardness should be performed in order to find processing methods to produce parts with uniform properties.
- Investigate material composition and grain structure with advanced microscopy, for example with SEM.
- The samples investigated was produced in a single row, multi-layer setup. In order to fully appreciate the process method effectiveness and the produced quality, further analysis should be performed with larger samples.

References

[1] J. D. Levin, "The economics of internet markets," National Bureau of Economic Research, Working Paper 16852, 2011-03. DOI: 10.3386/w16852. [Online]. Available: http://www.nber.org/papers/w16852.

[2] W. W. Wits, J. R. R. Garcıa, and J. M. J. Becker, "How additive manufacturing enables more sustainable end-user maintenance, repair and overhaul (mro) strategies," *Procedia Cirp*, vol. 40, pp. 693–698, 2016.

[3] M. Jakob and T. Qorri, "Additive manufacturing for maintenance, repair and operations within the aerospace industry at gkn," M.S. thesis, Chalmers University of Technology, 2021. eprint: https://hdl.handle.net/20.500.12380/302602.

[4] M. Prause, "Challenges of industry 4.0 technology adoption for smes: The case of japan," *Sustainability*, vol. 11, no. 20, p. 5807, 2019-10, ISSN: 2071-1050. DOI: 10.3390/su11205807. [Online]. Available: http://dx.doi.org/10.3390/su11205807.

[5] T. E. of Encyclopaedia Britannica, Ed., *single crystal*, 1998. [Online]. Available: https://www.britannica.com/science/single-crystal (visited on 2024-01-12).

[6] K. P. Rohrbach, "Trends in high temperature alloys: Selection and manufacture," *Aircraft Engineering and Aerospace Technology*, vol. 70, no. 3, pp. 209–214, 1998-06. DOI: 10.1108/00022669810693549. [Online]. Available: https://doi.org/10.1108/00022669810693549.

[7] M. J. Donachie and S. J. Donachie, *Superalloys, A Technical Guide*, Second. ASM International.

[8] R. C. Reed, *The Superalloys, Fundamentals and Applications*. Cambridge University Press, 2006.

[9] J. Belan, "Gcp and tcp phases presented in nickel-base superalloys," *Materials Today: Proceedings*, vol. 3, no. 4, pp. 936–941, 2016, 32nd DANUBIA ADRIA SYMPOSIUM on Advanced in Experimental Mechanics, ISSN: 2214-7853. DOI: https://doi.org/10.1016/j.matpr.2016.03.024. [Online]. Available: https://www.sciencedirect.com/science/article/pii/S2214785316002297.

[10] E. Nembach and G. Neite, "Precipitation hardening of superalloys by ordered ϒ-particles," *Progress in Materials Science*, vol. 29, no. 3, pp. 177–319, 1985-01. DOI: 10.1016/0079-6425(85)90001-5. [Online]. Available: https://doi.org/10.1016/0079-6425(85)90001-5.

[11] W. D. C. Jr and D. G. Rethwisch, *Callister's Materials Science and Engineering*. John Wiley & Sons, Incorporated, 2020, ISBN: 978-1-119-45391-8.

[12] F. Hanning, "Weld cracking of precipitation hardening ni-based superalloys, Investigation of repair welding characteristics and susceptibility towards strain age cracking," Ph.D. dissertation, Chalmers University of Technology, ISBN: 978-91-7905-258-4.

[13] K. Angelos, A. Alexandratou, A. Kladis, S. Deligiannis, P. Tsakiridis, and G. Fourlaris, "Comparative study of microstructural evolution and mechanical properties of inconel ® 718 and waspaloy ® welds," *MATEC Web of Conferences*, vol. 349, p. 02 004, 2021-01. DOI: 10.1051/matecconf/202134902004.

[14] S. Utada, R. Sasaki, R. C. Reed, and Y. T. Tang, "Overheating of waspaloy: Effect of cooling rate on flow stress behavior," *Materials & Design*, vol. 221, p. 110 911, 2022-09. DOI: 10.1016/j.matdes.2022.110911. [Online]. Available: https://doi.org/10.1016/j.matdes.2022.110911.

[15] *Haynes® waspaloy alloy*, H-3232, Datasheet, "Haynes® International", 2017. [Online]. Available: https://haynesintl.com/docs/default-source/pdfs/new-alloy-brochures/high-temperature-alloys/brochures/waspaloy.pdf?sfvrsn=e77229d4_26 (visited on 2024-01-08).

[16] J. Andersson, "Review of weldability of precipitation hardening ni- and fe-ni-based superalloys.," in *Proceedings of the 9th International Symposium on Superalloy 718 & Derivatives: Energy, Aerospace, and Industrial Applications*, Cham: Springer International Publishing, 2018, pp. 899–916, ISBN: 978-3-319-89480-5. DOI: 10.1007/978-3-319-89480-5_60.

[17] Q. Wei, Y. Xie, Q. Teng, M. Shen, S. Sun, and C. Cai, "Crack types, mechanisms, and suppression methods during high-energy beam additive manufacturing of nickel-based superalloys: A review," *Chinese Journal of Mechanical Engineering: Additive Manufacturing Frontiers*, vol. 1, no. 4, p. 100 055, 2022-12. DOI: 10.1016/j.cjmeam.2022.100055. [Online]. Available: https://doi.org/10.1016/j.cjmeam.2022.100055.

[18] J. F. S. Markanday, "Applications of alloy design to cracking resistance of additively manufactured ni-based alloys," *Materials Science and Technology*, vol. 38, no. 16, pp. 1300–1314, 2022. DOI: 10.1080/02670836.2022.2068759. eprint: https://doi.org/10.1080/02670836.2022.2068759. [Online]. Available: https://doi.org/10.1080/02670836.2022.2068759.

[19] W. J. Oh, Y. Son, and D. S. Shim, "Effect of in-situ heat treatments on deposition characteristics and mechanical properties for repairs using laser melting deposition," *Journal of Manufacturing Processes*, vol. 58, pp. 1019–1033, 2020. DOI: 10.1016/j.jmapro.2020.08.074.

[20] B. A. Rancurel, "Investigation of high temperature stability of additive manufactured austenitic stainless steels for space applications," M.S. thesis, Luleå University of Technology, 2023. eprint: urn:nbn:se:ltu:diva-99004.

[21] K. Kanishka and B. Acherjee, "A systematic review of additive manufacturing-based remanufacturing techniques for component repair and restoration," *Journal of Manufacturing Processes*, vol. 89, pp. 220–283, 2023. DOI: 10.1016/j.jmapro.2023.01.034.

[22] K. V. Wong and A. Hernandez, "A review of additive manufacturing," *International Scholarly Research Notices*, vol. 2012, 2012. DOI: 10.5402/2012/208760.

[23] M. Aliakbari, "Additive manufacturing: State-of-the-art, capabilities, and sample applications with cost analysis," M.S. thesis, KTH Royal Institute of Technology, 2012. eprint: urn:nbn:se:kth:diva-103598.

[24] B. Graf, S. Ammer, A. Gumenyuk, and M. Rethmeier, "Design of experiments for laser metal deposition in maintenance, repair and overhaul applications," *Procedia CIRP*, vol. 11, pp. 245–248, 2013-12. DOI: 10.1016/j.procir.2013.07.031.

[25] K. Säfsten and M. Gustavsson, *Research Methodology, For engineers and other problem-solvers*, 1:1. Studentlitteratur AB, 2020, ISBN: 978-91-44-12230-4.

[26] H. Snyder, "Literature review as a research methodology: An overview and guidelines," *Journal of Business Research*, vol. 104, pp. 333–339, 2019, ISSN: 0148-2963. DOI: https://doi.org/10.1016/j.jbusres.2019.07.039. [Online]. Available: https://www.sciencedirect.com/science/article/pii/S0148296319304564.

[27] *Secotom-10, Instruction manual*, 15037001, Struers A/S, 2010-06-01. [Online]. Available: https://www.struers.com/-/media/Library/Instruction-Manuals/Discontinued-combined/Secotom-10.pdf?dmc=1&ts=20200817T0648527865&lm=20200211T153049Z (visited on 2023-11-03).

Table 8: *Process data used for manufacturing samples used in the analysis. The combination number is referenced in the analysis when referring to individual samples.*

Combination	Laser power [W]	Scanning speed [mm/s]	Powder feed [g/min]
1	1750	25	16
2	1150	25	16
3	1750	15	16
4	1150	15	16
5	1750	25	10
6	1150	25	10
7	1750	15	10
8	1150	15	10
9, 10, 11	1450	20	13

A Manufacturing data

Manufacturing was performed with a discrete six beam powder nozzle with 16 mm focus distance, utilising a 1 mm laser fiber with a power of 12 kW. Argon was used as a shielding gas with the flow 10 L/min, and as a powder feed gas with the flow 5 L/min.

During manufacturing the process parameters were varied according to Table 8 Plates used for substrates was 347 Stainless steel with dimensions 150 mm × 60 mm × 3 mm.

Powder feed calibrated with 10 g/min as 60% rpm, 13 g/min as 78 %rpm and 16 g/min as 95 %rpm.